doi:10.1016/j.jmb.2007.08.021 *J. Mol. Biol.* (2007) **xx**, xxx–xxx

JMB

Available online at www.sciencedirect.com
ScienceDirect

ELSEVIER

Structural and Kinetic Properties of Lumazine Synthase Isoenzymes in the Order Rhizobiales

Sebastián Klinke[1], Vanesa Zylberman[1], Hernán R. Bonomi[1], Ilka Haase[2], Beatriz G. Guimarães[3], Bradford C. Braden[4], Adelbert Bacher[5], Markus Fischer[2] and Fernando A. Goldbaum[1]*

[1]*Fundación Instituto Leloir, IIBBA-CONICET, C1405BWE, Buenos Aires, Argentina*

[2]*Institut für Biochemie und Lebensmittelchemie, Universität Hamburg, D-20146 Hamburg, Germany*

[3]*Laboratório Nacional de Luz Síncrotron, Caixa Postal 6192, CEP 13084-971, Campinas, SP, Brazil*

[4]*Department of Natural Sciences, Bowie State University, Bowie, MD 20715-9465, USA*

[5]*Lehrstuhl für Organische Chemie und Biochemie, Technische Universität München, D-85747 Garching, Germany*

Received 4 July 2007; received in revised form 6 August 2007; accepted 9 August 2007

Edited by M. Guss

6,7-Dimethyl-8-ribityllumazine synthase (lumazine synthase; LS) catalyzes the penultimate step in the biosynthesis of riboflavin in plants and microorganisms. This protein is known to exhibit different quaternary assemblies between species, existing as free pentamers, decamers (dimers of pentamers) and icosahedrally arranged dodecamers of pentamers. A phylogenetic analysis on eubacterial, fungal and plant LSs allowed us to classify them into two categories: Type I LSs (pentameric or icosahedral) and Type II LSs (decameric).

The Rhizobiales represent an order of α-proteobacteria that includes, among others, the genera *Mesorhizobium*, *Agrobacterium* and *Brucella*. Here, we present structural and kinetic studies on several LSs from Rhizobiales. Interestingly, *Mesorhizobium* and *Brucella* encode both a Type-I LS and a Type-II LS called RibH1 and RibH2, respectively. We show that Type II LSs appear to be almost inactive, whereas Type I LSs present a highly variable catalytic activity according to the genus. Additionally, we have solved four RibH1/RibH2 crystallographic structures from the genera *Mesorhizobium* and *Brucella*. The relationship between the active-site architecture and catalytic properties in these isoenzymes is discussed, and a model that describes the enzymatic behavior is proposed. Furthermore, sequence alignment studies allowed us to extend our results to the genus *Agrobacterium*. Our results suggest that the selective pressure controlling the riboflavin pathway favored the evolution of catalysts with low reaction rates, since the excess of flavins in the intracellular pool in Rhizobiales could act as a negative factor when these bacteria are exposed to oxidative or nitrosative stress.

Keywords: 6,7-dimethyl-8-ribityllumazine synthase; X-ray crystallography; riboflavin biosynthesis; order Rhizobiales; enzymology

**Corresponding author.* E-mail addresses: sklinke@leloir.org.ar; vzylberman@leloir.org.ar; hbonomi@leloir.org.ar; ilka.haase@chemie.uni-hamburg.de; beatriz@lnls.br; bbraden@bowiestate.edu; adelbert.bacher@ch.tum.de; markus.fischer@chemie.uni-hamburg.de; fgoldbaum@leloir.org.ar.

Abbreviations used: LS, 6,7-dimethyl-8-ribityllumazine synthase; NRP, 5-nitro-6-ribitylamino-2,4(1*H*,3*H*)-pyrimidinedione; PEG, polyethylene glycol; RibH1-Bab, structure of *Brucella abortus* RibH1 enzyme; RibH1-Bab-NRP, structure of *B. abortus* RibH1 bound to the substrate analogue inhibitor NRP; RibH1-Bme-NRP, structure of *Brucella melitensis* RibH1 bound to NRP; RibH2-Mlo-NRP, structure of *Mesorhizobium loti* RibH2 bound to NRP.

Please cite this article as: Klinke, S. *et al.*, Structural and Kinetic Properties of Lumazine Synthase Isoenzymes in the Order Rhizobiales, *J. Mol. Biol.* (2007), doi:10.1016/j.jmb.2007.08.021

Introduction

Riboflavin (vitamin B_2) is the precursor of flavin mononucleotide and flavin adenine dinucleotide—two key cofactors involved in a wide variety of redox processes. This vitamin is biosynthesized in plants, fungi and certain microorganisms. In contrast, animals lack the necessary enzymes to produce riboflavin and, thus, they must acquire it from dietary sources.

The biosynthetic pathway of riboflavin has been studied in some detail (Fig. 1).[1,2] We focus our attention on its penultimate step, which is catalyzed by the enzyme 6,7-dimethyl-8-ribityllumazine synthase (lumazine synthase; LS).

The structures of LSs from several species have been studied by X-ray crystallography, electron microscopy and small-angle X-ray scattering.[3–10] Although all of them present a characteristic pentameric moiety as a basic building block, different degrees of quaternary association are seen for the molecules in solution according to the species. The protein exists as free pentamers, decamers (dimers of pentamers) and icosahedrons (dodecamers of pentamers). Additionally, some LSs can form large capsids with unknown molecular structures under certain circumstances.[11]

The Rhizobiales represent an order of α-proteobacteria that includes, among others, the genera *Mesorhizobium* (which forms nitrogen-fixing symbiosis with legumes), *Agrobacterium* (a plant pathogen that transforms cells, integrating the transferred DNA into the plant genome) and *Brucella* (an animal and human intracellular pathogen). The main *Brucella* species and their hosts are *Brucella abortus* (cattle), *Brucella melitensis* (sheep and goats) and *Brucella suis* (hogs). Genomic sequences for these three closely related species have been recently determined.[12–14]

Rhizobiales bear a riboflavin biosynthetic pathway that presents LS isoenzymes. We have demonstrated that *Brucella* spp. express two proteins with sequence similarity to LS, namely, RibH1 and RibH2. The enzyme RibH2 is assembled as a decamer in solution,[15] shows only residual activity as LS and may have evolved for a different, yet undescribed function.[16] Next, we have demonstrated that *B. abortus* RibH1 is pentameric in solution and also shows very low LS catalytic activity.[17] The existence of two enzymes for the same putative function in a single microorganism had prompted us to investigate this occurrence in other species and to perform an exhaustive phylogenetic analysis of the LS family.[17] This analysis allowed us to postulate the existence of two types of eubacterial, fungal and plant LS: Type I LSs, the great majority of LSs studied to date, and Type II LSs, which are present only in some eubacteria that also have a Type-I LS. *Brucella* spp. RibH2 is a Type-II LS, whereas its homolog RibH1 belongs to the Type-I branch. Additionally, *Mesorhizobium loti* also encodes its own RibH1 and RibH2 enzymes, which were assigned as part of the Type-I and Type-II LSs, respectively (Table 1).[17] In contrast, *Agrobacterium tumefaciens* only encodes a Type-I LS that is called RibH.

Herein, we complement these findings by presenting the crystallographic structure of RibH1 from *B. abortus* and *B. melitensis*. Minor differences are seen in the primary structure of RibH1 in the three sequenced *Brucella* species, whereas RibH2 bears a 100% sequence identity among them; thus, we will refer to it as *Brucella* spp. RibH2 throughout this

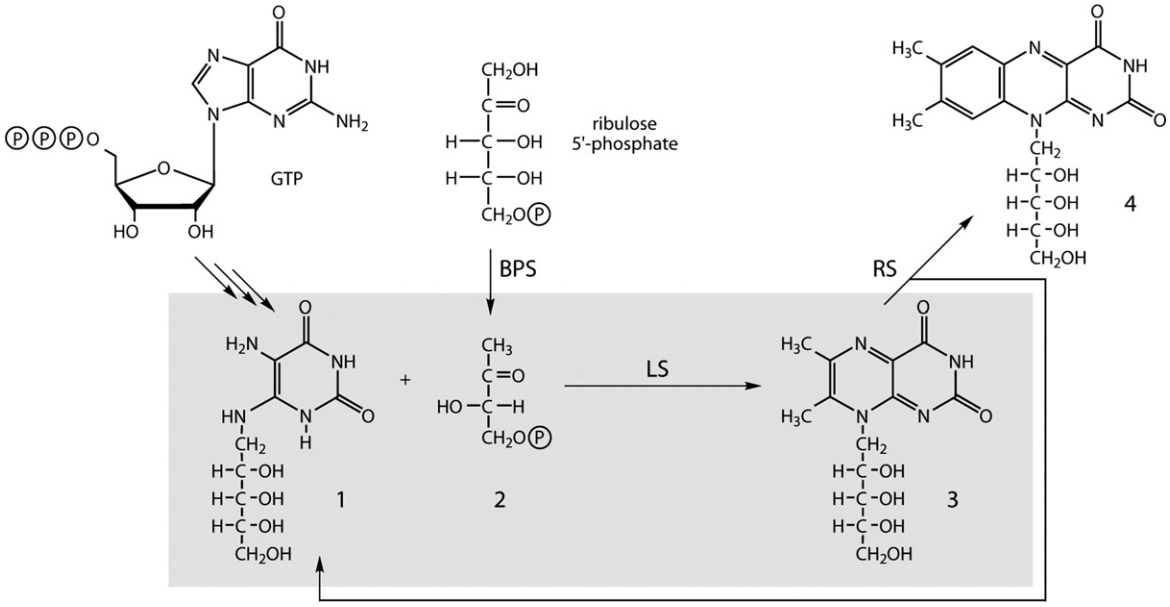

Fig. 1. Reactions involved in the riboflavin biosynthesis pathway. **1**, 5-Amino-6-ribitylamino-2,4(1*H*,3*H*)-pyrimidinedione; **2**, 3,4-dihydroxy-2-butanone 4-phosphate; **3**, 6,7-dimethyl-8-ribityllumazine; **4**, riboflavin; **BPS**, 3,4-dihydroxy-2-butanone 4-phosphate synthase; **LS**, 6,7-dimethyl-8-ribityllumazine synthase (reaction highlighted on gray background); **RS**, riboflavin synthase (dismutation reaction).

Please cite this article as: Klinke, S. *et al.*, Structural and Kinetic Properties of Lumazine Synthase Isoenzymes in the Order Rhizobiales, *J. Mol. Biol.* (2007), doi:10.1016/j.jmb.2007.08.021

Table 1. Main attributes of LSs in Rhizobiales

	Rhizobiales			
	Brucella		*Mesorhizobium*	
Attributes	Type I LS	Type II LS	Type I LS	Type II LS
Gene	RibH1	RibH2	RibH1	RibH2
Localization	Operon	Isolated	Operon	Isolated
Quaternary structure	Pentameric	Decameric	Studied here	
Enzymatic activity	Very low	Very low		

work. The three-dimensional (3D) models were solved either free or bound to 5-nitro-6-ribitylamino-2,4(1*H*,3*H*)-pyrimidinedione (NRP), a structural analogue of substrate **1** (see Figs. 1 and 3). A thorough comparison of these structures with that of *Brucella* spp. RibH2 and other LSs is presented.

We also describe the catalytic and structural properties of *M. loti* RibH1 and RibH2 proteins. All 3D structures solved in this work allowed us to perform a detailed analysis regarding LS catalytic activity and structure in *Brucella* and *Mesorhizobium* and to extend our results to the *Agrobacterium* genus, thus covering an important fraction of Rhizobiales. In this sense, we present a model that may explain why RibH1 from *M. loti* behaves catalytically like previously reported LSs, whereas its RibH2 protein and both RibH1 and RibH2 from *Brucella* are almost inactive as LSs.

Results and Discussion

Overall analysis and quality of crystallographic structures

We have solved four structures by X-ray crystallography in this work: *B. abortus* RibH1 (i) unliganded (RibH1-Bab) and (ii) bound to the substrate analogue inhibitor NRP (RibH1-Bab-NRP), and the complexes between NRP and (iii) *B. melitensis* RibH1 (RibH1-Bme-NRP) and (iv) *M. loti* RibH2 (RibH2-Mlo-NRP). All structures were solved by the molecular-replacement procedure as described in Materials and Methods. Good stereochemistry was observed in all cases, with >90% of the residues lying in the most favored region of their Ramachandran plots (Table 2). A single pentamer was found in the asymmetric units of RibH1-Bab, RibH1-Bab-NRP and RibH1-Bme-NRP, whereas two pentameric motifs are present in RibH2-Mlo-NRP in a head-to-head conformation to form a decamer. Therefore, a complete molecule was found in the asymmetric units of all structures, as will be discussed later. In all cases, there is lack of electron density in the first 5–11 residues at the N-termini. It is known that this region is highly flexible and, apart from icosahedral LSs in which they form a β strand, namely, β1,[4,7,9] these residues either are absent or show different conformations in the electron density of all non-icosahedral LS crystallographic structures available to date. The final $2F_o - F_c$ Fourier maps are consistent with the resolution and are continuous, with the exception of RibH1-Bab and RibH1-Bab-NRP, in which there is very weak electron density at the loop 85–91. In addition, RibH2-Mlo-NRP Gly42 residue from chain G is clearly disordered, being part of the G40–G44 loop that is in direct contact with a neighboring molecule in the crystal. RibH2-Mlo-NRP also lacks electron density for the last one to two C-terminal residues in each chain, as seen in the *Brucella* spp. RibH2 structure.[16] In the complex models, clear electron density for the ligand NRP was found in all active sites, which allowed its correct fitting both in position and in conformation. Additionally, several residues present poor or missing side-chain electron density in all structures and were modeled as alanine. In most cases, they correspond to exposed polar or charged residues. Crystallographic self-rotation functions calculated with CNS[18] show clear peaks at κ near 72°, supporting the pentameric architecture observed in the structures. It is important to note that the first cycles of refinement were done by applying restrained noncrystallographic symmetry to the models, considering each single chain as an equivalent region. During the last cycles, noncrystallographic symmetry restraints were not applied to let all monomers

Table 2. Refinement statistics of the final crystallographic models

Statistics	RibH1-Bab	RibH1-Bab-NRP	RibH1-Bme-NRP	RibH2-Mlo-NRP
Resolution limits (Å)	30.0–2.22	33.5–2.30	48.8–2.70	50.0–2.53
R-factor	0.242	0.217	0.210	0.213
R_{free}	0.287	0.241	0.271	0.281
Nonhydrogen protein atoms	5479	5463	5480	11,219
Nonhydrogen ligand atoms	–	105	105	210
Solvent molecules	181	219	87	219
Nonhydrogen ion atoms	5	6	6	45
R.m.s.d. bond lengths (Å)	0.006	0.006	0.007	0.007
R.m.s.d. bond angles (°)	1.15	1.21	1.24	1.41
Average *B*-factor (Å^2)	44.3	34.1	32.7	26.6
Ramachandran plot				
Most favored (%)	90.4	94.1	92.9	93.7
Additional allowed (%)	8.8	5.5	6.3	5.9
Generously allowed (%)	0.8	0.3	0.8	0.2
Disallowed (%)	–	–	–	0.2

Please cite this article as: Klinke, S. *et al.*, Structural and Kinetic Properties of Lumazine Synthase Isoenzymes in the Order Rhizobiales, *J. Mol. Biol.* (2007), doi:10.1016/j.jmb.2007.08.021

refine independently. The final average C^{α} root-mean-square deviations (r.m.s.d.), taking into account each chain individually, are 0.37 Å (RibH1-Bab), 0.22 Å (RibH1-Bab-NRP), 0.26 Å (RibH1-Bme-NRP) and 0.40 Å (RibH2-Mlo-NRP). As these values lie inside the experimental error for the working resolutions, we can confirm again that all structures presented here obey a strict 5-fold symmetry. From a formal point of view and considering the symmetry elements observed in the models, pentameric RibH1-Bab, RibH1-Bab-NRP and RibH1-Bme-NRP belong to the symmetry point group C5, whereas decameric RibH2-Mlo-NRP belongs to the D5 group. Detailed refinement statistics are shown in Table 2.

Description of RibH1-Bab structure

RibH1-Bab folds as a stable homopentamer, as presented in a previous work by our group.[17] Here, we further study this enzyme by describing its 3D crystallographic structure at 2.22 Å. Static light-scattering (SLS) experiments were also performed to complement the original data. In this sense, an average molecular weight (M_r) of 80,100 was determined (corresponding to 4.8 monomers), which is in good agreement with the 84,000 value calculated from its sequence.

The RibH1-Bab 16.8-kDa monomer structure closely resembles that of Type I eubacterial LSs.[17] Briefly, it consists of a 157-residue single domain that is composed of a central β sheet with four parallel strands, namely, β3β2β4β5. A total of five helices surround this β sheet: two on one side (α2α3) and three on the other (α1α4α5). Figure 2 shows the overall structure of RibH1-Bab, as well as its monomer architecture. α-Helices and β-strands are successively alternated along the polypeptide, giving rise to an overall β2α1β3α2β4α3β5α4α5 topology.[19] As mentioned before, the strand β1 is observed only in icosahedral LSs, being part of the central β sheet together with four strands of an adjacent subunit. The secondary structure elements in RibH1-Bab superimpose very well on those present in other LSs of known structure, with the exception of *Brucella* spp. RibH2, which will be discussed later. In contrast, there are clear differences in the arrangement of several loops that connect neighboring helices and strands. For example, the loop that joins α1 with β3 in RibH1-Bab is the shortest among all LSs described to date, comprising only the residues Gly42 and Ala43. A 3D alignment of all known family members (for an extensive analysis of sequence alignments, see Zylberman *et al.*[17]) shows the presence of one to four extra residues in that loop (*Mycobacterium tuberculosis* and *Schizosaccharomyces pombe* LS, respectively).[3,5]

Additionally, RibH1-Bab differs both in sequence and in conformation at the β hairpin that links α4 with α5, which is formed by four residues (Arg132, Glu133, Asp134 and Lys135) and is exposed to the solvent. Icosahedral LSs of known structure present there a highly conserved motif G(T/G)K(A/H)GN that is involved in a series of contacts with residues in helices α1 and α4 from a neighboring pentamer, thus stabilizing the capsid arrangement.[5] Insertions at this loop are known to be a determinant for the divergence in the quaternary assembly of this enzyme. In this sense, one to four extra residues are present in all known pentameric LSs. For example, *Saccharomyces cerevisiae* LS bears the insertion IDEA after the first glycine residue of the kink.[6] This gives rise to steric clashes both with its N-

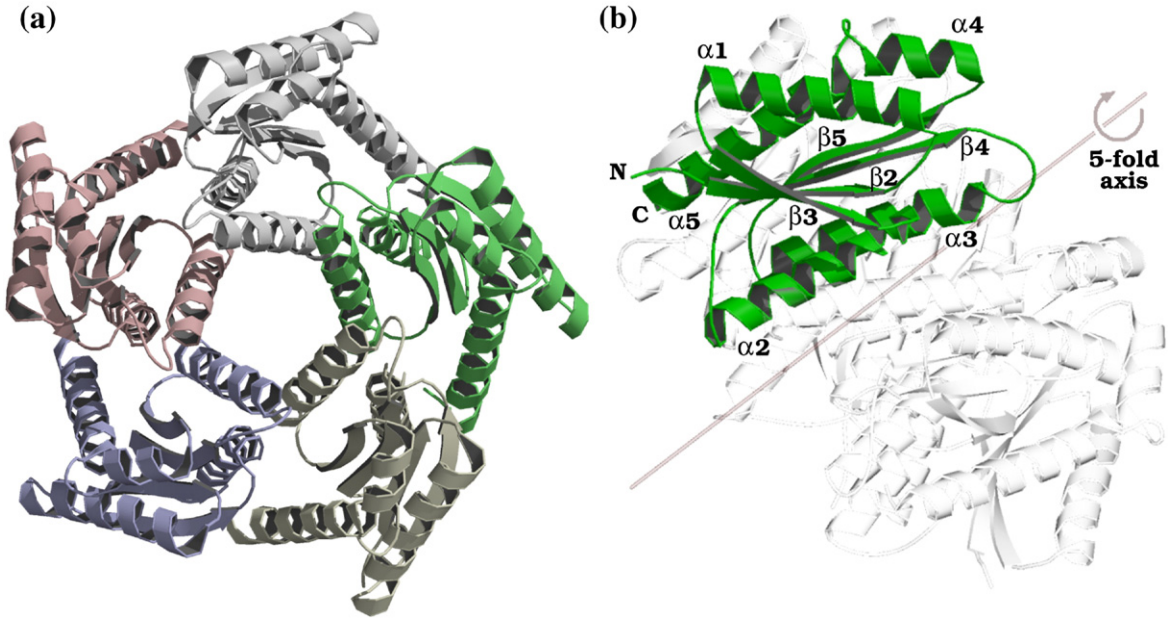

Fig. 2. RibH1-Bab structure. (a) Top view along the 5-fold noncrystallographic axis, with each monomer depicted in a different color. (b) Monomer architecture within the pentamer. Secondary structure elements are shown after *B. subtilis* LS nomenclature.[19] Polypeptide N- and C-termini are also marked.

Please cite this article as: Klinke, S. *et al.*, Structural and Kinetic Properties of Lumazine Synthase Isoenzymes in the Order Rhizobiales, *J. Mol. Biol.* (2007), doi:10.1016/j.jmb.2007.08.021

terminus and with residues in helix α4 when modeled as if the pentamers were arranged following an icosahedral symmetry similar to *Bacillus subtilis* LS. A comparable situation takes place in pentameric *Magnaporthe grisea* LS,[4] where the insertion VI would generate conflicts with N-terminal residues if the enzyme were icosahedrally assembled. In contrast to the observations mentioned before, RibH1-Bab is the first LS of known crystallographic structure that is arranged as a pentamer and bears no insertions in this loop. We will discuss below the reasons of this behavior. First, it is important to note that the structure of this β hairpin is unique among all known LSs, with residues Arg132–Lys135 being essentially nonsuperimposable on those present in the rest of the structures. There are basically two reasons for this: the occurrence of an arginine residue at position 131 and the ionic nature of the amino acids forming the loop. Residue 131 is the last member of helix α4 and is invariably glycine in all described LSs, with the exception of the *Brucella* spp. RibH2 enzyme (Asp) that is not considered in our analysis because it belongs to a different type of LS, as discussed later. The conformation of Arg131 in RibH1-Bab, with average torsion angles of $(\phi,\psi) = (-58°, 135°)$, clearly differs from that of the less constrained Gly131 in other structures (e.g., the average torsion angles are 72° and 22°, respectively, in *S. cerevisiae* LS). This generates a striking deviation of the main-chain path that affects the whole β hairpin. Additionally, the fact that all its residues are charged opens the chance to establish salt bridges that may stabilize the structure and conformation of the loop. Indeed, there are two key salt bridges: Arg131–Glu133 and Arg132–Asp32. These interactions are complemented with three hydrogen bonds that confer additional structural stability: Glu133-N–Glu133-$O^{\varepsilon 1}$, Asp134-N–Arg131-O and Lys135-N–Val128-O.

We propose that the main reason why RibH1-Bab folds as a pentamer and is unable to adopt a higher oligomerization state lies in this group of distinctive salt bridges. When RibH1-Bab pentamers are arranged following *B. subtilis* LS icosahedral architecture, no steric clashes are observed between the main-chain atoms of the neighboring pentameric moieties in the putative icosahedral structure. Nevertheless, severe collisions are seen in the α4–α5 β hairpin when all atoms are taken into account. Explicitly, Glu133 side chain would clash with that of Phe22 and the main chain of Asp24, and Arg131 side chain would sterically interfere with the main and side chains of Tyr23. The latter observation is valid for all five chains of the enzyme. Although these clashes might be avoidable at first sight by shifting the side-chain orientation in these residues, this would result in the break of the highly stabilizing Arg131–Glu133 salt bridge. Minor changes in the main-chain conformation due to this strict side-chain rearrangement might also disrupt the rest of the key interactions mentioned before, affecting the stability of the whole particle.

It is also important to note that the occurrence of a proline among the first 10 residues in all known pentameric LSs has been proposed to be a major determinant of their quaternary assembly.[4,6] Indeed, the conformational restrictions caused by its presence have been shown to affect the orientation of the N-terminus, which becomes unable to associate as the fifth strand of the β sheet (as seen in icosahedral LSs) and also leads to steric clashes when the pentameric particles that present electron density in this region are modeled as icosahedrons. RibH1-Bab is the first LS of known pentameric structure that lacks a proline residue in that zone. In contrast, a proline is found at position 13 just before strand β2 begins. To date, its influence on the quaternary structure of the enzyme is unknown. Unfortunately, electron density is absent for the first 10–11 residues in RibH1-Bab, which impedes a proper comparison with other LSs.

In conclusion, although we propose the loss of putative salt bridges as the main reason for the lack of an icosahedral arrangement, the N-terminus conformation effects cannot be ruled out as a further element that defines the pentameric quaternary association for RibH1-Bab.

Studies on the active site of RibH1-Bab

Pentameric assembly of LS subunits is of vital importance for catalytic activity, since the active site of this enzyme is located in all cases at the interface between adjacent monomers, involving residues from both chains.[19] RibH1-Bab, as well as all documented LSs, assembles a pentamer in which the five α3 helices interact with each other and face the center of the particle, generating a superhelical left-handed coiled coil around the 5-fold axis (see Fig. 2a).

The topologically equivalent active sites of LS (5 in the case of pentamers and 60 in the case of icosahedral particles) are deep clefts with high exposure to the solvent and specific binding sites for both substrates involved in the reaction. In order to provide a better understanding of the RibH1-Bab active site, in terms of both ligand recognition and architecture, we have crystallized and solved the structure of this protein bound to the substrate analogue inhibitor NRP (RibH1-Bab-NRP).

The RibH1-Bab active site resembles that of the previous LSs studied. One monomer contributes residues from three different regions: Phe22 and Tyr23 (loop after β2), Gly52–Glu55 (loop after β3) and Thr82–Val94 (part of β4 and α3 and the loop that joins them). Additionally, the neighboring monomer participates with residues Asn115′–Leu118′ (strand β5) and the side chains of His129′ (helix α4), Lys135′ (β hairpin connecting α4 and α5), and Lys137′ and Phe140′ (helix α5).

The ligand NRP bears a single chemical modification with respect to the natural pyrimidinedione substrate **1**, that being the presence of a nitro group instead of an amino linked to its aromatic ring (see Fig. 3). This inhibitor binds to the active site of

Please cite this article as: Klinke, S. *et al.*, Structural and Kinetic Properties of Lumazine Synthase Isoenzymes in the Order Rhizobiales, *J. Mol. Biol.* (2007), doi:10.1016/j.jmb.2007.08.021

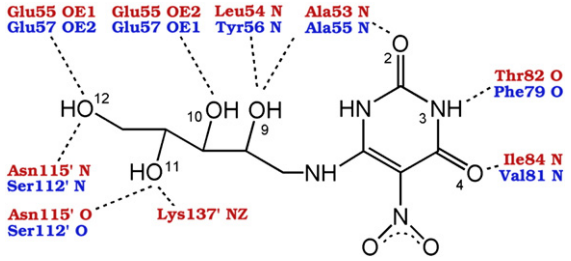

Fig. 3. Schematic representation of the hydrophilic interactions between NRP and LS in the complex structures RibH2-Mlo-NRP (residue atoms in blue) and RibH1-Bab-NRP and RibH1-Bme-NRP (residue atoms in red). The contact with residue Lys137′ is only valid in RibH1-Bab-NRP. Numbers near the ligand atoms correspond to the nomenclature used in the Protein Data Bank structures.

B. abortus RibH1 in a way similar to that observed in several complexed LSs described before.[3–7,20] Ligand recognition is carried out by a series of hydrophobic and hydrophilic interactions with residues of two neighboring subunits. Polar contacts comprise hydrogen bonds between atoms O_2, N_3 and O_4 from NRP and the main-chain amides and carbonyl groups of the enzyme. The ribityl moiety of the ligand is also hydrogen-bonded to several main-chain atoms, to the Lys137′ amino group and to the carboxyl $O^{\varepsilon 1}$ and $O^{\varepsilon 2}$ atoms of residue Glu55, which is highly conserved among LSs. Water molecules linking atom O_2 in NRP and main-chain groups of the protein are also observed. Figure 3 summarizes the polar interactions mentioned before.

A strong hydrophobic environment at both sides of the aromatic ring of NRP complements its recognition by the enzyme. The main contact is performed by the residue Phe22, whose side chain adopts a parallel conformation with respect to the pyrimidine ring of the ligand with a separation of 3.5 Å. This coplanar π–π interaction is always found in complexed LSs and is of key importance, with position 22 being occupied either by a Phe residue (icosahedral LSs) or by a Trp residue (pentameric LSs) in almost all sequences known to date. Surprisingly, RibH1-Bab is the first LS of known 3D structure that assembles as a pentamer and presents a phenylalanine residue at this position. In addition to Phe22, aromatic side chains of Phe140′ and Tyr23 give rise to an "aromatic shield" on top of the ligand. Below its pyrimidine ring, side chains of residues Ala53, Leu54, Val83 and Val94 complement the nonpolar environment at the substrate **1**-binding site. A comparison between RibH1-Bab and RibH1-Bab-NRP models reveals no major differences in the overall structure of the enzyme. The average C^{α} r.m.s.d., taking into account each monomer separately, is only 0.51 Å.

The substrate **2**-binding site comprises the region that is most exposed to the solvent in the active site of LS. Due to the fact that this compound is relatively unstable,[21] there are no crystallographic structures available to fully describe its specific recognition. Nevertheless, several models of LS complexed either with analogues bearing phosphonated alkyl moieties or with inorganic phosphate present in their mother liquors allow the precise binding site of the phosphate group of substrate **2** (see Fig. 1) to be determined. This group is usually linked to amide nitrogen atoms of residues present in the loop that joins β4 with α3. However, its main contact takes place by means of a salt bridge with an arginine or a histidine residue. A basic amino acid in this position (position 129 in RibH1-Bab numbering) is highly conserved among LSs, with >90% of the known sequences bearing an arginine. RibH1-Bab presents a histidine residue in that position, with clear electron density on the Fourier map. The fact that the mother liquor both in RibH1-Bab and in RibH1-Bab-NRP contains an appreciable amount of calcium chloride (0.2 M) has made it impossible to add inorganic phosphate to the crystallization condition. As such, no electron density is seen at the phosphate-binding site. However, a 3D superposition of RibH1-Bab-NRP and *S. pombe* LS complexed with the same ligand[5] (average C^{α} r.m.s.d. = 1.42 Å) shows that residue His129 is located and oriented in a proper conformation to bind the phosphate group of substrate **2** at the active site (Fig. 4). The presence of intact binding sites for both substrates of the reaction is a main attribute of Type I eubacterial, fungal and plant LSs, in contrast to Type II LSs, as will be discussed later in this work.

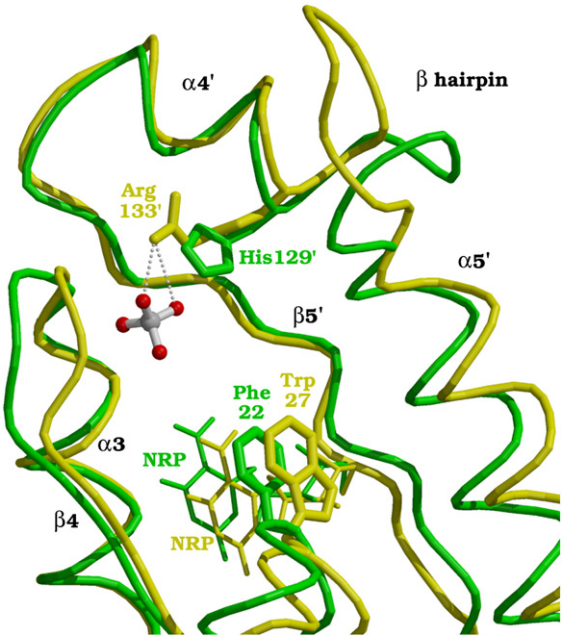

Fig. 4. Superposition of the active sites of the complex structures RibH1-Bab-NRP (green) and *S. pombe* LS-NRP (yellow). The substrate analogue inhibitor is drawn with slim lines. The interaction between the phosphate group and the side chain of residue Arg133′ (both from the *S. pombe* enzyme) is depicted with dotted lines. Note that two neighboring subunits are involved in the recognition of NRP and the phosphate ion.

Please cite this article as: Klinke, S. *et al.*, Structural and Kinetic Properties of Lumazine Synthase Isoenzymes in the Order Rhizobiales, *J. Mol. Biol.* (2007), doi:10.1016/j.jmb.2007.08.021

Structural comparison between LSs RibH1 and RibH2 from *B. abortus*

The determination of the 3D structure of RibH1-Bab opens a new perspective to understanding this family of enzymes, as this is the first time that two LSs encoded by a single organism are fully described in terms of their crystallographic structures. Before genomes of *B. abortus*, *B. melitensis* and *B. suis* were sequenced,[12–14] the existence of RibH1 was unknown. On the other hand, RibH2 had been discovered before and had been thought to be the actual LS of *Brucella* spp. and, thus, the enzyme responsible for that function in the cell. However, a relatively low LS catalytic activity was observed,[22] and clear differences were noted in the crystallographic structure of RibH2 in comparison with previous known LSs,[15,23] even before RibH1 was discovered. This led to the hypothesis that RibH2 might perform a different function in the cell, although conserving a residual LS activity.[16] Recently, an exhaustive phylogenetic analysis[17] allowed us to classify RibH2 as a member of a new distinctive family of LSs—that of the Type-II eubacterial LSs.

Figure 5 shows a superposition of the monomers of RibH1 and RibH2 from *B. abortus*. Despite the low sequence identity (only 21%), both polypeptides superimpose well, with an average C^{α} r.m.s.d. of 1.50 Å for 128 C^{α} aligned. Nevertheless, clear differences are seen in two regions. Helix α2 is one turn longer and deviates away from the central β sheet in RibH1-Bab (see Fig. 5b). Additionally, the region that begins at the end of strand β5 and finishes at the β hairpin diverges in both models. As shown in Fig. 5a, RibH2 presents a longer strand β5, followed by a pronounced loop that places helix α4 about 30° shifted with respect to the one in RibH1. This shift, along with a special residue insertion where all the other known LSs present a β hairpin, leads to an undistorted 32-residue-long α4 helix that extends up to the C-terminus of the RibH2 polypeptide. This difference has been proposed to be a determinant for the novel decameric arrangement of RibH2 in *Brucella* spp.[16] Additionally, this striking variation in both the secondary and the tertiary structures of the polypeptide chain leads to the absence of a positively charged residue (like His129 as seen, e.g., in RibH1) that is able to contact the phosphate group of substrate **2** in RibH2. Thus, the presence of a distorted binding site for this substrate has been proposed as the main reason for the very low catalytic activity observed in RibH2.[16]

Finally, the fact that both RibH1 and RibH2 have also been solved bound to the ligand NRP allows the possibility to compare its recognition between them. In this sense, all contacts are very well conserved, with the exception of Lys137′-N^{ζ}-NRP-O11 in RibH1-Bab-NRP. In the RibH2 complex, its related residue (Lys135′) places its side chain >6 Å away from the ribityl moiety of the inhibitor.

Crystallographic and enzymatic studies on RibH1 from *B. melitensis*

As noted before, all sequenced *Brucella* species, namely, *B. abortus*, *B. melitensis* and *B. suis*, encode a RibH2 enzyme with a 100% sequence identity. On the other hand, minor but important differences are observed in RibH1 between these three members. For example, *B. melitensis* RibH1 presents a single difference in a key residue of the active site with respect to the *B. abortus* enzyme, which is the occurrence of an arginine residue at position 129 instead of a histidine (see Fig. 6). Next, *B. suis* RibH1 also shows a second amino acid exchange at position 2, bearing an aspartate residue instead of

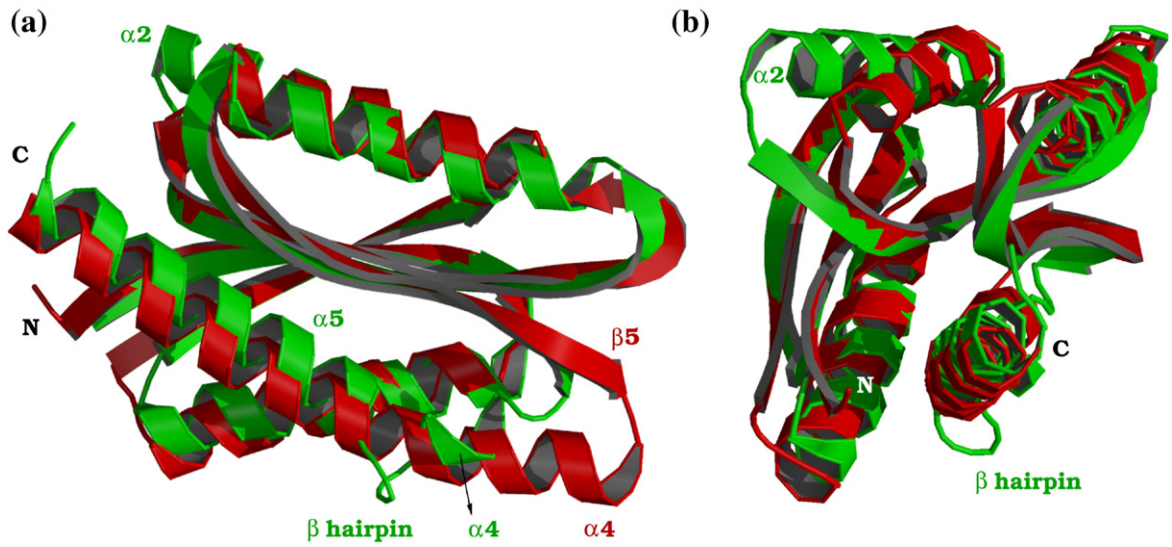

Fig. 5. Superposition of the monomers from RibH1 (green; this work) and RibH2 (red; Protein Data Bank accession code 1DI0[23]) from *B. abortus*. Key elements of the structures are marked. (a) Front view emphasizing the α/β/α sandwich topology of both polypeptides and the differences in the β5–α4 region. (b) Left view highlighting a longer and displaced α2 helix in RibH1-Bab.

Please cite this article as: Klinke, S. *et al.*, Structural and Kinetic Properties of Lumazine Synthase Isoenzymes in the Order Rhizobiales, *J. Mol. Biol.* (2007), doi:10.1016/j.jmb.2007.08.021

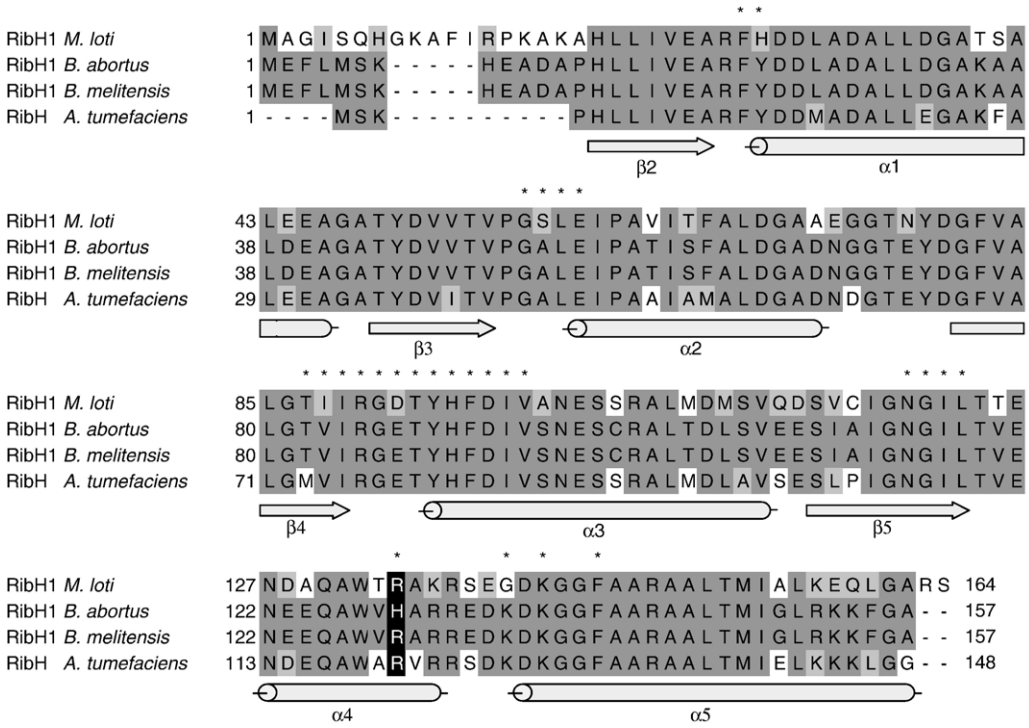

Fig. 6. Amino acid sequence alignment of Type I RibH1 from *M. loti*, *B. abortus* and *B. melitensis*, and of Type I RibH from *A. tumefaciens*. Identical residues are marked with dark-gray background, whereas light gray is used for conserved substitutions with respect to *B. abortus* and *B. melitensis* RibH1. Elements of secondary structure are presented below the sequences, and residues belonging to the active site are marked with stars. Differences at the active site residue 129 (after *B. abortus* and *B. melitensis* numbering) are highlighted on a black background.

a glutamate that is observed in the other two sequences. Since this region is highly flexible, the latter conservative change is thought not to affect the properties of this enzyme at all. However, the divergence at residue 129 may be of importance in terms of structure and catalytic activity, since the majority of LSs bear an arginine residue in this position, as stated before. For this reason, we have crystallized and solved the 3D structure of *B. melitensis* RibH1 bound to the inhibitor NRP (RibH1-Bme-NRP).

The enzyme is a homopentamer as expected. SLS experiments yielded an average M_r of 75,300, which corresponds to 4.5 monomers, in reasonable concordance with the calculated M_r of 84,000. The RibH1-Bme-NRP structure clearly resembles that of RibH1-Bab-NRP. The average C^{α} r.m.s.d. is very low—0.40 Å when isolated monomers are considered and 0.53 Å for the whole pentamers. In contrast to RibH1-Bab and RibH1-Bab-NRP, there is a clear and definite electron density in the loop 85–91 in the *B. melitensis* enzyme, but the reason for this behavior remains unclear. When the active sites of RibH1-Bme-NRP and *S. pombe* LS bound to the same ligand are superimposed as in Fig. 4, both key arginine residues (residue 129 in *B. melitensis* and residue 133 in *S. pombe*) overlap almost perfectly. This is a sign of an intact phosphate-binding site in RibH1-Bme-NRP. The inhibitor shows the same contact pattern as in RibH1-Bab-NRP but lacks the salt bridge between Lys137′ and the ribityl side chain of NRP (see Fig. 3). As noted above, the same situation takes place in RibH2.

Table 3 shows the catalytic parameters of RibH1 from *B. melitensis*, as well as other enzymes studied in this work. The influence of the His129→Arg mutation on the catalytic activity of RibH1 from both *Brucella* species will be discussed later.

Table 3. Enzymatic parameters and quaternary structure for all enzymes studied in this work

Enzyme	K_m (μM)		k_{cat} (s^{-1})	k_{cat}/K_m (M^{-1} s^{-1})		Source	Quaternary structure	3D structure available (source)
	Substrate **1**	Substrate **2**		Substrate **1**	Substrate **2**			
RibH1 *B. abortus*	90±16	125±10	0.005±0.001	56±16	40±8	17	Pentameric	Yes (this study)
RibH1 *B. melitensis*	4±2	225±40	0.003±0.001	700±630	12±7	This study	Pentameric	Yes (this study)
RibH1 *M. loti*	2.5±1.0	15±4	0.040±0.003	16,000±7500	2700±900	This study	Pentameric	No
RibH2 *Brucella* spp.	10	4000	0.006±0.001	600	1.5	16	Decameric	Yes (16,23)
RibH2 *M. loti*	20±10	450±100	$<3\times10^{-4}$	<14	<0.7	This study	Decameric	Yes (this study)

Please cite this article as: Klinke, S. *et al.*, Structural and Kinetic Properties of Lumazine Synthase Isoenzymes in the Order Rhizobiales, *J. Mol. Biol.* (2007), doi:10.1016/j.jmb.2007.08.021

Quaternary structure and enzymatic analysis of RibH1 and RibH2 from *M. loti*

M. loti is an α2-proteobacterium that is phylogenetically related to *Brucella*, whose main function is related to nitrogen fixation in plants. Despite their two unrelated hosts, *M. loti* also encodes both RibH1 and RibH2 enzymes in its genome. We have cloned and expressed both proteins in order to compare their quaternary structure and catalytic parameters with those from *Brucella*.

SLS experiments yielded an average M_r of 85,500 for RibH1, in excellent agreement with a theoretical pentameric M_r of 86,000. Next, SLS experiments on RibH2 showed an average M_r of 158,500 (corresponding to 9.2 monomers), in good concordance with the calculated decameric M_r of 173,000. In conclusion, both *M. loti* RibH1 and RibH2 present the same quaternary arrangement as in *Brucella*. Nevertheless, these results are not surprising, since interspecies sequence identity is 68% for RibH1 and 61% for RibH2. Figures 6 and 7 show the sequence alignment of RibH1 and RibH2 in both genera, respectively.

Table 3 also presents the enzymatic parameters of both LSs from *M. loti*. As we will discuss later, all these results are in fair agreement with the Type-I/Type-II LS phylogenetic analysis proposed in our previous work.[17]

Three-dimensional structure analysis on RibH2 from *M. loti*

In this study, we also solved the structure of RibH2 from *M. loti* bound to NRP (RibH2-Mlo-NRP) to compare it with the closely related *Brucella* spp. RibH2 model. As SLS experiments anticipated, the crystallographic structure of the *M. loti* protein is decameric, being assembled as a head-to-head-oriented dimer of pentamers as in the *Brucella* spp. enzyme (Fig. 8). Thus, the RibH2-Mlo-NRP structure corresponds to the second decameric LS to have ever been described. As expected, a detailed structural alignment search against the whole Protein Data Bank database shows *Brucella* spp. RibH2 as first hit, with C^{α} r.m.s.d. of 0.68 Å for monomers, 0.75 Å for isolated pentamers and 0.85 Å for the full molecule. Therefore, both structures superimpose almost perfectly, although there are minor differences in the loop that connects α1 and β3.

As described in a previous study,[16] one of the most important features in the stabilization of the decameric quaternary structure of *Brucella* spp. RibH2 is a series of aromatic stacking contacts between histidine residues belonging to different pentamers at the equatorial interface of the protein. A total of 15 contacts are seen: His119–His120′ (5), His120–His119′ (5) and His121a–His121a′ (5). *M. loti* RibH2 presents an asparagine residue at position 119 (position 120 in *Brucella*), thus losing 10 out of these 15 interactions. Nevertheless, this protein has evolved to develop a new structural solution for enhanced stability: two new interpentameric salt bridges are seen between residues Arg128–Glu132′ and Glu132–Arg128′ in four of the five chains, giving rise to eight new strong contacts that connect both pentamers.

The ligand is recognized in RibH2-Mlo-NRP exactly in the same way as in *Brucella* spp. RibH2.[16] Trp21 stacks the pyrimidine ring of the inhibitor at a distance of 3.6 Å. Figure 3 complements the information about NRP binding.

The residues that compose the active site of *M. loti* RibH2 are almost the same as in the *Brucella* spp. enzyme, with a few conservative replacements that do not affect the binding pocket of both substrates. As such, Ile82, Asp83 and Asp90 in *Brucella* spp. RibH2 are Val81, Asn82 and Glu89 in the *M. loti*

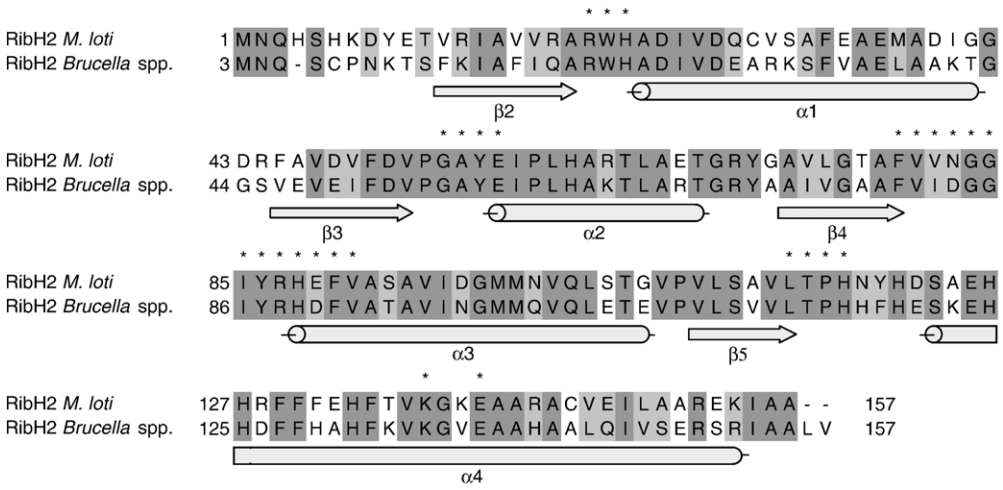

Fig. 7. Sequence alignment of Type II RibH2 from *M. loti* and *Brucella* spp. Background colors and secondary structure elements are depicted as in Fig. 6. *Brucella* spp. RibH2 special numbering, which begins at position 3 and presents four residues at position 121 (121, 121a, 121b and 121c), was adopted as published[23] to maintain sequence identity with the *B. subtilis* LS[7] and is also kept in all *Brucella* spp. RibH2 crystallographic structures solved (Protein Data Bank accession codes 1DI0, 1T13 and 1XN1).[16,23]

Please cite this article as: Klinke, S. *et al.*, Structural and Kinetic Properties of Lumazine Synthase Isoenzymes in the Order Rhizobiales, *J. Mol. Biol.* (2007), doi:10.1016/j.jmb.2007.08.021

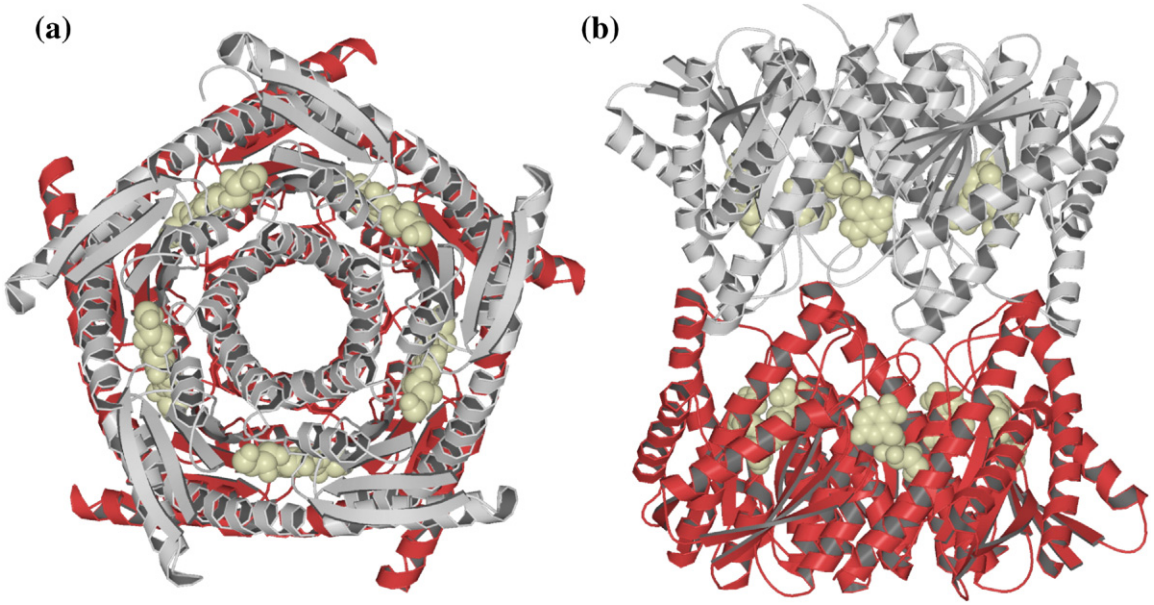

Fig. 8. RibH2-Mlo-NRP structure. Each pentamer is drawn in a different color, and the inhibitor molecules (10) are represented as space-filling models in yellow. (a) View along the 5-fold axis. (b) Front view highlighting the pentamer–pentamer interface and the overall spool shape of the enzyme.

enzyme, respectively. In order to study the binding site of substrate **2**, RibH2-Mlo-NRP was crystallized in the presence of 20 mM inorganic phosphate coming from the final dialysis buffer. Weak electron density was found in the last cycles of refinement in nine of the active sites at the putative binding pocket of the phosphate group of substrate **2**. For this reason, these peaks were assigned as phosphate ions in the final model. Their positions and binding mode are similar to those found in the *Brucella* spp. RibH2 enzyme.

Influence of the active-site architecture on catalytic activity: focus on the special *Brucella* case

To conclude, we analyze in close detail the enzymatic parameters presented in Table 3. The value of the kinetic constant K_m of substrate **1** resembles that of the previously studied LSs in both *M. loti* and *Brucella* enzymes because its binding site is very well conserved among all types of LSs of known structure, as noted before. Nevertheless, there is a clear divergence in the case of *B. abortus* RibH1 (90 μM). This value is about 1 order of magnitude higher than that usually observed (i.e., 8.6 μM in *B. subtilis* LS and 5.0 μM in *S. pombe* LS).[24,25] The RibH1-Bab-NRP structure does not show any special feature that could explain this fact; moreover, its related RibH1-Bme-NRP structure (which only differs at Arg129, a residue that does not contact NRP) presents a "standard" K_m of 4 μM.

With respect to the K_m of substrate **2**, both RibH2 present the highest values seen for LSs. The evolution of Type II LSs to assemble as decamers *via* an extended α4-helix architecture affects its binding site as noted above. There is lack of a proper salt bridge interaction with an Arg or a His residue. On the other side, *M. loti* RibH1 shows a K_m of 15 μM, which is in the same order as those seen in Type I and archaeal LSs (e.g., 55 μM in Type I *B. subtilis* LS and 52 μM in archaeal *Methanococcus jannaschii* LS).[24,26] Although its 3D structure has not been determined yet, key position 134 (which corresponds to position 129 in *B. abortus* and *B. melitensis* RibH1; see Fig. 6) presents an arginine residue that is believed to be responsible for substrate **2** binding. Next, both *B. abortus* and *B. melitensis* RibH1 show a lower K_m with respect to Type II LSs, due to the presence of His129 and Arg129, respectively. However, both K_m values are slightly higher than in the rest of the Type-I and archaeal LSs investigated. It is interesting to note that we had expected a lower K_m value for *B. melitensis* RibH1 in comparison with the *B. abortus* enzyme. At first sight, the presence of its arginine residue, which presents a greater net positive charge than a histidine and a longer side chain, would have been able to bind the phosphate group of substrate **2** with a stronger affinity.

Finally, remarkable results regarding the turnover number k_{cat} in RibH1 and RibH2 were observed in both genera studied. *Brucella* spp. and *M. loti* RibH2 clearly present lower values than Type I and archaeal LSs (i.e., 0.056 s^{-1} in *B. subtilis* and 0.023 s^{-1} in *M. jannaschii*).[24,26] Moreover, the *M. loti* enzyme is almost inactive. The partially distorted active-site architecture of Type II LSs is the basis of this behavior, as discussed earlier. On the other hand, *M. loti* RibH1 presents catalytic efficiencies (k_{cat}/K_m) for both substrates that are a few orders of magnitude greater than those seen in all enzymes in Table 3. Indeed, we can affirm that it behaves as an "ordinary" Type-I LS, with catalytic parameters in the same order of magnitude as those seen in other active LSs.

Surprisingly, both *B. abortus* and *B. melitensis* RibH1 are enzymes with an unexpected low k_{cat},

Please cite this article as: Klinke, S. *et al.*, Structural and Kinetic Properties of Lumazine Synthase Isoenzymes in the Order Rhizobiales, *J. Mol. Biol.* (2007), doi:10.1016/j.jmb.2007.08.021

which is even smaller than that of RibH2 in the same bacteria. In order to arrive at a possible explanation for this unusual performance, we focused our analysis on a special region of the active site (residues 129–137) and compared it with all known LSs. There are three key residues whose side chain points towards the cleft: Arg/His129, Lys137 and Lys135 (Fig. 9b). The role of residue 129 has already been analyzed. Next, residue Lys137 has been proposed by Zhang *et al.* to be a major determinant in the correct positioning and binding of a phosphonated intermediate compound during the reaction.[20] This study was performed on *Aquifex aeolicus* LS, whose Lys135 residue superimposes almost perfectly on *Brucella* RibH1 Lys137. This latter residue, a histidine in some sequences, is always linked *via* a salt bridge to an aspartate or a glutamate in its vicinity in all LSs studied (Glu138 in Fig. 9a and c). This pair has been proposed to reorientate during the reaction course in a cooperative manner to "pull" this phosphonated intermediate to afford the following product (a Schiff base) in a correct *cis* configuration. It is important to note that all *Brucella* RibH1 enzymes lack the counterpart of Lys137, as Phe140, rather than a Glu or an Asp, is found in this position (see Fig. 9b). The absence of this important pair may affect the catalytic activity of this enzyme. However, we cannot propose this as the main reason for the low k_{cat} in *Brucella*, since *M. loti* RibH1, which catalyzes the reaction with much better performance, presents the same aromatic residue (Phe145) instead of an acidic one.

On the other hand, residue Lys135 is unique for *Brucella* RibH1 among all known LSs. It is part of its distinctive β hairpin; thus, a 3D superposition with all LSs of known structure shows no basic residues in that particular region of the active site. The occurrence of three positive amino acids close to each other (see Fig. 9b and d) may generate severe

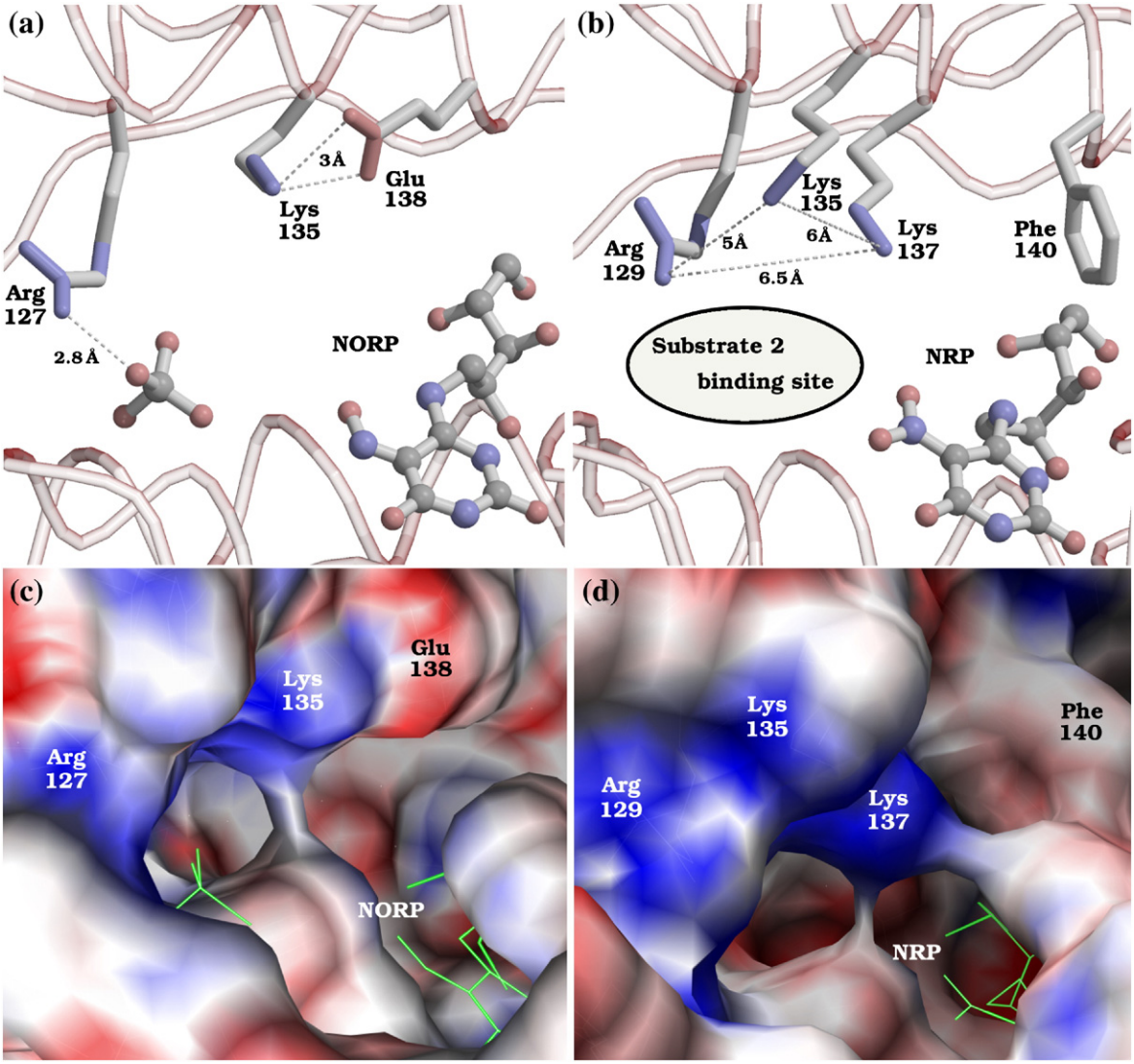

Fig. 9. Focus on the influence of positive residues on the active site of LS. (a) *A. aeolicus* LS complexed with 5-nitroso-6-ribitylamino-2,4(1*H*,3*H*)-pyrimidinedione (NORP) and inorganic phosphate. (b) RibH1-Bme-NRP. Average distances between the charged groups are presented. The side chain of Phe140 (a residue infrequently seen in LSs at this position) is also drawn. (c and d) Electrostatic surface analysis of the structures shown above.

Please cite this article as: Klinke, S. *et al.*, Structural and Kinetic Properties of Lumazine Synthase Isoenzymes in the Order Rhizobiales, *J. Mol. Biol.* (2007), doi:10.1016/j.jmb.2007.08.021

charge repulsions during the course of the reaction that may lead to a reduced catalytic activity in *Brucella*. This observation is in agreement with the absence of a basic residue in this particular position in *M. loti* RibH1, which is a glycine (Gly140). The positive environment generated by Lys135 may also be responsible for the slightly higher K_m values observed for substrate **2** in both *B. abortus* and *B. melitensis* RibH1 enzymes.

Then, taking into account the sequence alignment in Fig. 6, we predict *A. tumefaciens* RibH to be an LS of very low catalytic activity, since it presents the same positive triad Arg–Lys–Lys as in *B. melitensis* RibH1, with a 76% sequence identity.

It is important to note that the only remarkable difference in the active site of RibH2 from *Brucella* spp. and *M. loti* is the absence of His/Arg129, since, like almost all LSs, they bear the distinctive basic–acidic pair Lys135–Glu138 (after *Brucella* spp. numbering; see Fig. 7) and they do not present the positive triad mentioned before. This supports again the idea that the very low catalytic activities of the RibH2 enzymes may lie in the absence of a basic residue that binds substrate **2**.

To conclude, we discard any negative influence of other residues of the active site on the catalytic parameters, particularly the region near His90 (according to *Brucella* RibH1 numbering, which has been proposed to act as a proton-transfer agent during the reaction), since sequence identity between *A. tumefaciens* RibH and *M. loti* and *Brucella* RibH1 enzymes is quite good there, with a few conservative substitutions that most likely do not affect the structure of the catalytic cleft on these LSs.

Conclusions

The four crystallographic structures and the kinetic and biophysical studies presented here are well in line with the phylogenetic analysis and the Type-I/Type-II LS family classification we had proposed in our previous study.[17] For the first time, two RibH1–RibH2 pairs were characterized both in structure and in catalytic properties.

In summary, the structural elements that dictate the different quaternary structures in LSs from Rhizobiales are quite distinct from those described previously in other species. In this sense, pentameric RibH1 from the genus *Brucella* shows a characteristically smaller and charged loop at the region that links α4 with α5, which may preclude the assembly of this protein into an icosahedral particle. Next, we have demonstrated that both RibH2 from *Brucella* spp. and *M. loti* form decameric assemblies based on the absence of the abovementioned loop and the occurrence of an undistorted, 32-residue-long helix α4. In the RibH2 pentameric moieties, the N-termini of the five α4 helices and the loops that connect them with the contiguous β5 strands make a protuberant surface that fits tightly into the neighboring pentamer to form a decameric particle. Although the general assembly of the equatorial interface is very similar in both cases studied, *M. loti* RibH2 shows a noteworthy variation in the nature of the interpentameric contacts, as salt bridges stabilize the decameric structure rather the than aromatic stacking interactions between His residues that are observed in *Brucella* spp. RibH2.

Regarding the enzymatic properties, we have shown that *Mesorhizobium* bears a fully active LS (RibH1) and an almost inactive LS (RibH2), whereas in *Brucella*, both enzymes have very low catalytic activity, although for different reasons. On this basis, the unique RibH to *Agrobacterium* is therefore proposed to also exhibit a very low catalytic activity. This unusual scenario suggests that the selective pressure controlling this pathway favored the evolution of catalysts with low reaction rates. In fact, riboflavin is required in small amounts only, and excess production could unnecessarily deplete the precursor pools, namely, Guanosine triphosphate and ribulose 5′-phosphate. Moreover, an excess of flavins in the intracellular pool in Rhizobiales could act as a negative factor when these bacteria are exposed to oxidative or nitrosative stress. In this sense, Rhizobiales regulate iron concentration by sensing the physiological consequence of metal availability, rather than its concentration *per se*, and thus provide for more flexible regulation.[27,28]

The question of which selective pressures could have prevented the loss of the *RibH2* gene or could have favored its more recent acquisition by horizontal gene transfer is still open to answer. Interestingly, the Type-II LS is an immunodominant antigen of *B. abortus*, and knockout mutants for this protein have shown a marked decrease in survival and virulence (Marchesini *et al.*, unpublished results). As in the case of *Brucella*, *M. loti* RibH2 has almost no activity as LS and would be regulated by a riboswitch that senses flavin mononucleotide,[29] suggesting that the Type-II LSs may have evolved into very poor catalysts or, alternatively, to harbor a new, as-yet-unknown function.

Materials and Methods

Materials

NRP was obtained as described by published procedures.[30] Genomic DNAs of *B. melitensis* and *M. loti* were kindly provided by Dr. Angeles Zorreguieta (Fundación Instituto Leloir) and Dr. Rodolfo Ugalde (IIB-UNSAM), respectively.

Gene cloning

B. abortus RibH1 gene was cloned into the expression plasmid pT7-7 as described.[17] *B. melitensis RibH1* gene, as well as *M. loti RibH1* and *RibH2* genes, was amplified by PCR using their respective chromosomal DNAs as template and the oligonucleotides presented in Table 4 as primers. The three amplicons were digested with NdeI and BamHI and were then ligated into the plasmid pET11a (Novagen, Madison, WI), which had been treated

Please cite this article as: Klinke, S. *et al.*, Structural and Kinetic Properties of Lumazine Synthase Isoenzymes in the Order Rhizobiales, *J. Mol. Biol.* (2007), doi:10.1016/j.jmb.2007.08.021

Table 4. Oligonucleotides used for PCR amplification of *B. melitensis RibH1* and *M. loti RibH1* and *RibH2* genes

Designation	Sequence	Restriction sites
RibH1 B. melitensis	F: 5′ ATAATAATACATATGGAGTTTCTCATGTCCAAGCA 3′	NdeI (CA*TATG)
	R: 5′ TATTATTATAAGGATCCTTATCAGGCTCCGAATTTTTTG 3′	BamHI (G*GATCC)
RibH1 M. loti	F: 5′ ATAATAATACATATGGCTGGTATATCCCAACACGGC 3′	NdeI
	R: 5′ TATTATTATAAGGATCCTTATCACGATCGGGCTCCCAAT 3′	BamHI
RibH2 M. loti	F: 5′ ATAATAATACATATGAATCAGCATTCCCACAAAGACTAT 3′	NdeI
	R: 5′ TATTATTATAAGGATCCTTATCATGCCGCGATCTTTTC 3′	BamHI

F, oligonucleotide used as forward primer; R, oligonucleotide used as reverse primer.

with the same restriction enzymes. All constructions were checked by DNA sequencing following the method of Sanger *et al.*[31] *Escherichia coli* BL21(DE3) competent cells (Stratagene, La Jolla, CA) were transformed with the resulting ligation mixtures.

Protein expression

In all cases, recombinant cells were grown at 37 °C overnight in 25 ml of LB medium containing 100 μg/ml ampicillin, with agitation (250 rpm). These preparations were diluted to 500 ml and grown to an absorbance (600 nm) of 1.0. At this time, the cultures were induced by the addition of isopropyl-β-D-thiogalactopyranoside to a final concentration of 1 mM and incubated further for 4 h at 37 °C, with agitation (250 rpm). The bacteria were centrifuged at 10,000*g* for 8 min at 4 °C.

Protein purification

After expression, different strategies were followed according to the particular protein. *B. abortus*, *B. melitensis* and *M. loti* RibH1 bacterial pellets were suspended and sonicated in a solution containing 50 mM sodium/potassium phosphate (pH 7.0) and 5 mM EDTA (buffer A). Preparations were centrifuged at 25,000*g* for 20 min at 4 °C, and the insoluble fractions were discarded. Cytoplasm fractions were dialyzed overnight against buffer A and then purified by anion-exchange chromatography in a fast protein liquid chromatography apparatus using a Q-Sepharose column (all columns by GE Healthcare, Piscataway, NJ) equilibrated with buffer A. RibH1 fractions were eluted using a linear gradient of 0–1.5 M sodium chloride in buffer A (buffer B). The proteins were further purified by gel-filtration chromatography in a Superdex 200 column with isocratic elution in phosphate-buffered saline containing 0.5 M sodium chloride. The appropriate fractions were then dialyzed against buffer A and loaded in a Mono-Q column equilibrated with the same buffer. Highly purified RibH1 proteins were eluted with a linear gradient of 0–1.5 M sodium chloride in buffer A (buffer B). It is important to note that three different columns were needed in all cases to separate proteins mostly from nonproteic contaminants. The final products were then dialyzed against crystallization buffer [10 mM Tris (pH 7.10) and 25 mM sodium chloride], concentrated by ultracentrifugation to ~10 mg/ml with Centricon YM-10 concentrators (Millipore, Billerica, MA) and stored at −20 °C.

For *M. loti* RibH2, the bacterial pellets were suspended and sonicated in a solution containing 50 mM Tris (pH 8.0) and 5 mM EDTA. After centrifugation, the cytoplasm fraction was dialyzed overnight against 50 mM Tris (pH 8.5; buffer C) and then loaded in a Q-Sepharose column equilibrated with buffer C. RibH2 fractions were eluted using a linear gradient of 0–1 M sodium chloride in buffer C (buffer D) and further purified by gel filtration (Superdex 200 column) in a similar manner to the RibH1 enzymes. Finally, RibH2 fractions were dialyzed against buffer C and loaded in a Mono-Q column equilibrated with the same buffer. RibH2 fractions were eluted with a linear gradient of 0–1 M sodium chloride in buffer C (buffer D), dialyzed against crystallization buffer [20 mM sodium/potassium phosphate (pH 7.10) and 25 mM sodium chloride], concentrated to ~10 mg/ml and stored at −20 °C.

The purity of all protein preparations was checked by 15% SDS polyacrylamide gels and UV spectrophotometry.

Crystallization

All crystals were grown by means of the hanging-drop vapor-diffusion method at 19 °C. Round-shaped RibH1-Bab crystals of about 0.30 mm × 0.20 mm × 0.10 mm dimension were obtained after several days with a mother liquor consisting of 12% (wt/vol) polyethylene glycol (PEG) 4000, 0.1 M Hepes (pH 7.7) and 0.2 M calcium chloride. RibH1-Bab-NRP crystals were grown with 18% (wt/vol) PEG 400, 0.1 M Mes (pH 6.6) and 0.2 M calcium chloride in the presence of a 5-fold molar excess of the substrate analogue inhibitor NRP. Sharp-edged prisms of about 0.30 mm × 0.25 mm × 0.10 mm dimension were found after a week. RibH1-Bme-NRP crystals were grown in a similar manner, with 22% (wt/vol) PEG 400, 0.1 M Mes (pH 6.3) and 0.2 M calcium chloride as mother liquor, yielding crystals that are comparable in shape and slightly reduced in size after a week. Finally, prism-shaped RibH2-Mlo-NRP crystals of 0.15 mm × 0.15 mm × 0.05 mm dimension were also obtained by cocrystallization with 16% (wt/vol) PEG 4000, 0.1 M ammonium sulfate and 15% isopropanol after several days.

Diffraction data collection and processing

RibH1-Bab and RibH1-Bab-NRP datasets were collected at the D03B-MX1 Beamline at the Laboratório Nacional de Luz Síncrotron (Campinas, Brazil)[32] using a MarCCD 165 detector (Mar USA, Evanston, IL). RibH1-Bme-NRP and RibH2-Mlo-NRP diffraction data were collected at the X9A Beamline at the National Synchrotron Light Source, Brookhaven National Laboratory (New York), also using a MarCCD 165 detector. Crystals were soaked in cryoprotectant solutions consisting of a mother liquor supplemented with 15% (wt/vol) PEG 400 (RibH1-Bab and RibH2-Mlo-NRP), 30% (wt/vol) PEG 400 (RibH1-Bab-NRP) and 12% (wt/vol) PEG 400 (RibH1-Bme-NRP), and flash-cooled in a 100-K nitrogen stream. A single crystal was used for the collection of each dataset. X-ray diffraction data were indexed and integrated with MOSFLM, scaled using SCALA and converted to amplitudes with

Please cite this article as: Klinke, S. *et al.*, Structural and Kinetic Properties of Lumazine Synthase Isoenzymes in the Order Rhizobiales, *J. Mol. Biol.* (2007), doi:10.1016/j.jmb.2007.08.021

TRUNCATE. All these programs are part of the CCP4 package.[33] RibH1-Bab crystals diffracted to a maximum resolution of 2.22 Å and belonged to the monoclinic space group *C*2. RibH1-Bab-NRP and RibH1-Bme-NRP crystals diffracted to 2.30 and 2.70 Å, respectively, in the trigonal space group $P3_221$. Finally, RibH2-Mlo-NRP crystals diffracted to 2.53 Å, belonging also to the space group *C*2. In all cases, 5% of the measured reflections were flagged for cross-validation purposes. Details on data collection parameters and processing statistics are shown in Table 5.

Structure solution, model building and refinement

All structures were solved using the molecular-replacement method with the program AMoRe.[34] The RibH1-Bab-NRP structure was solved using a pentameric block of the icosahedral LS from *B. subtilis* (Protein Data Bank accession code 1RVV) as search model.[7] To reduce bias, this model was modified by removing the first 50 residues in each chain due to the low sequence identity between both proteins in this region and by mutating all nonconserved residues to alanine. Five solutions were found inside the asymmetric unit after rotation and translation steps (15–4.0 Å), which correspond to the same unique solution rotated 72° from each other coaxially to the 5-fold crystallographic axis of the protein. After checking for a consistent packing in the crystal lattice, the oriented model was then subjected to rigid body refinement in CNS[18] (8–3.6 Å), considering each chain as a separate entity. Next, a cycle of simulated annealing refinement applying restrained noncrystallographic symmetry was performed in CNS (8–3.2 Å), yielding a model with *R*-factor = 0.463 and R_{free} = 0.479. Double- and single-difference Fourier maps built at this stage showed clear electron density for several side chains, which were modeled using the program O.[35] Further cycles of simulated annealing refinement using all reflections gradually up to the diffraction limit (2.30 Å) yielded maps that allowed the reconstruction of the main chain before residue 50 and almost all side chains that had been replaced by alanine. A strong and well-defined electron density was found inside each active site, which corresponds to the bound substrate analogue inhibitor NRP. Coordinates of this ligand were obtained from the Protein Data Bank entry 1KYY (*S. pombe* LS complexed with NRP)[5] and manually fit into the density, followed by several cycles of positional and isotropic *B*-factor refinement using the maximum-likelihood algorithm. In the last cycles, noncrystallographic symmetry restraints were relaxed, allowing each chain to refine independently. The model was completed with solvent molecules and a few calcium ions that were found near aspartate or glutamate residues, with most of them bridging neighboring molecules.

The final RibH1-Bab-NRP structure, without solvent molecules and ligand coordinates, was successfully used as search model for the resolution of RibH1-Bab and RibH1-Bme-NRP. In the latter complex, a special search model was built, with residue 129 mutated to alanine. The refinement and manual building procedures were, in both cases, similar to the ones applied for RibH1-Bab-NRP.

The RibH2-Mlo-NRP structure was solved using a pentamer from *Brucella* spp. RibH2 as search model (Protein Data Bank entry 1T13),[16] with all nonconserved residues mutated to alanine. A total of two pentamers were found in the asymmetric unit, facing each other in a head-to-head conformation as expected. The model was refined and built in a similar manner to the other structures. In the final cycles of refinement, electron density was found in almost all putative binding sites of the phosphate group of substrate **2**, which was interpreted as bound phosphate ions coming from the crystallization buffer.

In all structures, only reflections satisfying the condition $F \geq 2\sigma$ were included in the refinement. The topology and

Table 5. X-ray data collection parameters and processing statistics

Parameters	RibH1-Bab	RibH1-Bab-NRP	RibH1-Bme-NRP	RibH2-Mlo-NRP
Data collection				
Number of frames	127	194	100	160
Wavelength (Å)	1.438	1.438	0.9794	0.9794
Indexing and scaling				
Cell parameters (Å)				
a	124.10	95.32	97.65	154.38
b	68.52	95.32	97.65	122.22
c	90.65	171.74	175.40	94.93
Cell angles (°)				
α	90	90	90	90
β	108.40	90	90	125.43
γ	90	120	120	90
Space group	*C*2	$P3_221$	$P3_221$	*C*2
Resolution limit (Å)	2.22	2.30	2.70	2.53
Number of unique reflections	31,466	40,562	22,473	46,386
Multiplicity[a]	2.7 (2.6)	9.5 (7.9)	3.9 (2.2)	3.4 (3.1)
I/σ	12.3 (2.6)	10.5 (2.2)	5.8 (2.2)	9.7 (2.9)
R_{merge} (%)[b]	4.1 (28.2)	5.6 (34.0)	10.0 (31.3)	7.4 (25.5)
Completeness (%)	94.8 (88.7)	99.5 (97.0)	85.0 (82.3)	96.7 (89.2)
Pentamers/asymmetric unit	1	1	1	2
Solvent content (%)	43.0	53.7	56.8	41.3
Matthews coefficient ($Å^3$/Da)	2.2	2.7	2.9	2.1
B-factor (Wilson plot; $Å^2$)	43.1	39.7	54.6	39.4

[a] Values in parentheses correspond to the highest resolution shell: RibH1-Bab, 2.34–2.22 Å; RibH1-Bab-NRP, 2.42–2.30 Å; RibH1-Bme-NRP, 2.85–2.70 Å; RibH2-Mlo-NRP, 2.66–2.53 Å.

[b] $R_{merge} = [\Sigma_i | I_i - \langle I \rangle | / \Sigma_i I_i]$.

Please cite this article as: Klinke, S. *et al.*, Structural and Kinetic Properties of Lumazine Synthase Isoenzymes in the Order Rhizobiales, *J. Mol. Biol.* (2007), doi:10.1016/j.jmb.2007.08.021

parameter files needed for the refinement of the ligand NRP in the complex structures were obtained from the HIC-Up database.[36] The final refinement statistics are found in Table 2.

SLS measurements

The average molecular weight in solution of all proteins presented in this work was calculated with a Precision Detectors PD2080 Static Light Scattering instrument (Precision Detectors, Bellingham, MA) linked to a fast protein liquid chromatography apparatus and an LKB 2142 differential refractometer (LKB, Bromma, Sweden). In each case, 500 μl of a ~0.5-mg/ml protein solution was injected into a Superdex 200 column and eluted with phosphate-buffered saline containing 0.5 M sodium chloride. Both signals corresponding to 90° light scattering ($\lambda = 682$ nm) and the refractive index of the peaks eluted were recorded and then processed with the Discovery32 software supplied by Precision Detectors. Bovine serum albumin ($M_r = 66{,}500$) was used as standard for light-scattering detector calibration.

Determination of enzymatic parameters

LS enzymatic activity was determined as described previously.[21,24,37] Briefly, a series of mixtures containing the enzyme, 100 mM potassium phosphate (pH 7.0), 5 mM EDTA and various concentrations of substrates **1** and **2** were prepared. Generation of 6,7-dimethyl-8-ribityllumazine (product **3**) was monitored photometrically at $\lambda = 410$ nm and 37 °C. The resulting data were fitted to the Michaelis–Menten equation or to the Hill equation. Due to the appreciable nonenzymatic generation of product,[38] reaction mixtures without enzyme were used to correct the experimental data.

Sequence alignments

Sequences were aligned using the program ClustalW, version 1.83,[39] at the European Bioinformatics Institute homepage† (Figs. 6 and 7).

Evaluation of the models and graphical representation

All 3D structures presented here were validated with the programs PROCHECK[40] and SFCHECK.[41] Superpositions and r.m.s.d. calculations were done with the Protein Structure Comparison Service SSM at the European Bioinformatics Institute.[42] Figures were generated with MOLSCRIPT,[43] Raster3D,[44] Chimera[45] and ChemDraw (CambridgeSoft, Cambridge, MA). Electrostatic surface calculations were performed with the program APBS.[46]

Protein Data Bank depositions

Atomic coordinates and structure factors were deposited in the RCSB Protein Data Bank under accession codes 2F59 (RibH1-Bab-NRP), 2I0F (RibH1-Bab), 2O6H (RibH1-Bme-NRP) and 2OBX (RibH2-Mlo-NRP).

† www.ebi.ac.uk

Acknowledgements

This work was supported by a Howard Hughes Medical Institute international grant to F.A.G. and by a grant from the Agencia Nacional de Promoción Científica y Tecnológica. We were also supported by the Fonds der Chemischen Industrie, the Hans-Fischer-Gesellschaft eV and the Laboratório Nacional de Luz Síncrotron (projects MX1-3342 and MX1-4420).

M.F. and F.A.G. acknowledge Bundesministerium für Bildung und Forschung's and Secretaría de Ciencia y Tecnológia's support for exchange visits between laboratories (project ARG 04/Z06). S.K. would also like to thank Dr. Robert M. Sweet and Dr. Zbigniew Dauter for their help during X-ray diffraction data collection at the Rapidata 2006 course. The use of the National Synchrotron Light Source, Brookhaven National Laboratory, was supported by the U.S. Department of Energy, Office of Science, Office of Basic Energy Sciences, under contract no. DE-AC02-98CH10886.

References

1. Fischer, M. & Bacher, A. (2005). Biosynthesis of flavocoenzymes. *Nat. Prod. Rep.* **22**, 324–350.
2. Fischer, M. & Bacher, A. (2006). Biosynthesis of vitamin B_2 in plants. *Physiol. Plant.* **126**, 304–318.
3. Morgunova, E., Meining, W., Illarionov, B., Haase, I., Jin, G., Bacher, A. *et al.* (2005). Crystal structure of lumazine synthase from *Mycobacterium tuberculosis* as a target for rational drug design: binding mode of a new class of purinetrione inhibitors. *Biochemistry*, **44**, 2746–2758.
4. Persson, K., Schneider, G., Jordan, D. B., Viitanen, P. V. & Sandalova, T. (1999). Crystal structure analysis of a pentameric fungal and an icosahedral plant lumazine synthase reveals the structural basis for differences in assembly. *Protein Sci.* **8**, 2355–2365.
5. Gerhardt, S., Haase, I., Steinbacher, S., Kaiser, J. T., Cushman, M., Bacher, A. *et al.* (2002). The structural basis of riboflavin binding to *Schizosaccharomyces pombe* 6,7-dimethyl-8-ribityllumazine synthase. *J. Mol. Biol.* **318**, 1317–1329.
6. Meining, W., Mörtl, S., Fischer, M., Cushman, M., Bacher, A. & Ladenstein, R. (2000). The atomic structure of pentameric lumazine synthase from *Saccharomyces cerevisiae* at 1.85 Å resolution reveals the binding mode of a phosphonate intermediate analogue. *J. Mol. Biol.* **299**, 181–197.
7. Ritsert, K., Huber, R., Turk, D., Ladenstein, R., Schmidt-Bäse, K. & Bacher, A. (1995). Studies on the lumazine synthase/riboflavin synthase complex of *Bacillus subtilis*: crystal structure analysis of reconstituted, icosahedral beta-subunit capsids with bound substrate analogue inhibitor at 2.4 Å resolution. *J. Mol. Biol.* **253**, 151–167.
8. Zhang, X., Meining, W., Fischer, M., Bacher, A. & Ladenstein, R. (2001). X-ray structure analysis and crystallographic refinement of lumazine synthase from the hyperthermophile *Aquifex aeolicus* at 1.6 Å resolution: determinants of thermostability revealed from structural comparisons. *J. Mol. Biol.* **306**, 1099–1114.

Please cite this article as: Klinke, S. *et al.*, Structural and Kinetic Properties of Lumazine Synthase Isoenzymes in the Order Rhizobiales, *J. Mol. Biol.* (2007), doi:10.1016/j.jmb.2007.08.021

9. Mortl, S., Fischer, M., Richter, G., Tack, J., Weinkauf, S. & Bacher, A. (1996). Biosynthesis of riboflavin. Lumazine synthase of *Escherichia coli*. *J. Biol. Chem.* **271**, 33201–33207.
10. Morgunova, E., Saller, S., Haase, I., Cushman, M., Bacher, A., Fischer, M. & Ladenstein, R. (2007). Lumazine synthase from *Candida albicans* as an antifungal target enzyme: structural and biochemical basis for drug design. *J. Biol. Chem.* **282**, 17231–17241.
11. Zhang, X., Konarev, P. V., Petoukhov, M. V., Svergun, D. I., Xing, L., Cheng, R. H. *et al.* (2006). Multiple assembly states of lumazine synthase: a model relating catalytic function and molecular assembly. *J. Mol. Biol.* **362**, 753–770.
12. DelVecchio, V. G., Kapatral, V., Redkar, R. J., Patra, G., Mujer, C., Los, T. *et al.* (2002). The genome sequence of the facultative intracellular pathogen *Brucella melitensis*. *Proc. Natl. Acad. Sci. USA*, **99**, 443–448.
13. Paulsen, I. T., Seshadri, R., Nelson, K. E., Eisen, J. A., Heidelberg, J. F., Read, T. D. *et al.* (2002). The *Brucella suis* genome reveals fundamental similarities between animal and plant pathogens and symbionts. *Proc. Natl. Acad. Sci. USA*, **99**, 13148–13153.
14. Halling, S. M., Peterson-Burch, B. D., Bricker, B. J., Zuerner, R. L., Qing, Z., Li, L. L. *et al.* (2005). Completion of the genome sequence of *Brucella abortus* and comparison to the highly similar genomes of *Brucella melitensis* and *Brucella suis*. *J. Bacteriol.* **187**, 2715–2726.
15. Zylberman, V., Craig, P. O., Klinke, S., Braden, B. C., Cauerhff, A. & Goldbaum, F. A. (2004). High order quaternary arrangement confers increased structural stability to *Brucella* sp. lumazine synthase. *J. Biol. Chem.* **279**, 8093–8101.
16. Klinke, S., Zylberman, V., Vega, D. R., Guimaraes, B. G., Braden, B. C. & Goldbaum, F. A. (2005). Crystallographic studies on decameric *Brucella* spp. Lumazine synthase: a novel quaternary arrangement evolved for a new function? *J. Mol. Biol.* **353**, 124–137.
17. Zylberman, V., Klinke, S., Haase, I., Bacher, A., Fischer, M. & Goldbaum, F. A. (2006). Evolution of vitamin B_2 biosynthesis: 6,7-dimethyl-8-ribityllumazine synthases of *Brucella*. *J. Bacteriol.* **188**, 6135–6142.
18. Brunger, A. T., Adams, P. D., Clore, G. M., Delano, W. L., Gros, P., Grosse-Kunstleve, R. W. *et al.* (1998). Crystallography and NMR system (CNS): a new software system for macromolecular structure determination. *Acta Crystallogr. Sect. D: Biol. Crystallogr.* **54**, 905–921.
19. Ladenstein, R., Schneider, M., Huber, R., Bartunik, H. D., Wilson, K., Schott, K. & Bacher, A. (1988). Heavy riboflavin synthase from *Bacillus subtilis*. Crystal structure analysis of the icosahedral β60 capsid at 3.3 Å resolution. *J. Mol. Biol.* **203**, 1045–1070.
20. Zhang, X., Meining, W., Cushman, M., Haase, I., Fischer, M., Bacher, A. & Ladenstein, R. (2003). A structure-based model of the reaction catalyzed by lumazine synthase from *Aquifex aeolicus*. *J. Mol. Biol.* **328**, 167–182.
21. Kis, K., Volk, R. & Bacher, A. (1995). Biosynthesis of riboflavin. Studies on the reaction mechanism of 6,7-dimethyl-8-ribityllumazine synthase. *Biochemistry*, **34**, 2883–2892.
22. Goldbaum, F. A., Velikovsky, C. A., Baldi, P. C., Mörtl, S., Bacher, A. & Fossati, C. A. (1999). The 18-kDa cytoplasmic protein of *Brucella* species—an antigen useful for diagnosis—is a lumazine synthase. *J. Med. Microbiol.* **48**, 833–839.
23. Braden, B. C., Velikovsky, C. A., Cauerhff, A. A., Polikarpov, I. & Goldbaum, F. A. (2000). Divergence in macromolecular assembly: X-ray crystallographic structure analysis of lumazine synthase from *Brucella abortus*. *J. Mol. Biol.* **297**, 1031–1036.
24. Fischer, M., Haase, I., Kis, K., Meining, W., Ladenstein, R., Cushman, M. *et al.* (2003). Enzyme catalysis *via* control of activation entropy: site-directed mutagenesis of 6,7-dimethyl-8-ribityllumazine synthase. *J. Mol. Biol.* **326**, 783–793.
25. Fischer, M., Haase, I., Feicht, R., Richter, G., Gerhardt, S., Changeux, J. P. *et al.* (2002). Biosynthesis of riboflavin: 6,7-dimethyl-8-ribityllumazine synthase of *Schizosaccharomyces pombe*. *Eur. J. Biochem.* **269**, 519–526.
26. Haase, I., Mortl, S., Kohler, P., Bacher, A. & Fischer, M. (2003). Biosynthesis of riboflavin in archaea. 6,7-Dimethyl-8-ribityllumazine synthase of *Methanococcus jannaschii*. *Eur. J. Biochem.* **270**, 1025–1032.
27. Rodionov, D. A., Gelfand, M. S., Todd, J. D., Curson, A. R. & Johnston, A. W. (2006). Computational reconstruction of iron- and manganese-responsive transcriptional networks in alpha-proteobacteria. *PLoS Comput. Biol.* **2**, e163.
28. Johnston, A. W., Todd, J. D., Curson, A. R., Lei, S., Nikolaidou-Katsaridou, N., Gelfand, M. S. & Rodionov, D. A. (2007). Living without Fur: the subtlety and complexity of iron-responsive gene regulation in the symbiotic bacterium *Rhizobium* and other alpha-proteobacteria. *Biometals*, **20**, 501–511.
29. Vitreschak, A. G., Rodionov, D. A., Mironov, A. A. & Gelfand, M. S. (2002). Regulation of riboflavin biosynthesis and transport genes in bacteria by transcriptional and translational attenuation. *Nucleic Acids Res.* **30**, 3141–3151.
30. Cresswell, R. M. & Wood, H. C. S. (1960). The biosynthesis of pteridines: Part I. The synthesis of riboflavin. *J. Chem. Soc.*, 4768–4775.
31. Sanger, F., Nicklen, S. & Coulson, A. R. (1977). DNA sequencing with chain-terminating inhibitors. *Proc. Natl. Acad. Sci. USA*, **74**, 5463–5467.
32. Polikarpov, I., Oliva, G., Castellano, E. E., Garratt, R. C., Arruda, P., Leite, A. & Craievich, A. (1998). The protein crystallography beamline at LNLS, the Brazilian National Synchrotron Light source. *Nucl. Instrum. Methods Phys. Res. Sect. A*, **405**, 159–164.
33. Collaborative Computational Project, Number 4 (1994). The CCP4 suite: programs for protein crystallography. *Acta Crystallogr. Sect. D: Biol. Crystallogr.* **50**, 760–763.
34. Navaza, J. A. C. (1994). AMoRe: an automated package for molecular replacement. *Acta Crystallogr. Sect. A*, **50**, 157–163.
35. Jones, T. A., Zou, J. Y., Cowan, S. W. & Kjeldgaard, M. (1991). Improved methods for the building of protein models in electron density maps and the location of errors in these models. *Acta Crystallogr. Sect. A*, **47**, 110–119.
36. Kleywegt, G. J. & Jones, T. A. (1998). Databases in protein crystallography. *Acta Crystallogr. Sect. D: Biol. Crystallogr.* **54**, 1119–1131.
37. Kis, K. & Bacher, A. (1995). Substrate channeling in the lumazine synthase/riboflavin synthase complex of *Bacillus subtilis*. *J. Biol. Chem.* **270**, 16788–16795.
38. Kis, K., Kugelbrey, K. & Bacher, A. (2001). Biosynthesis of riboflavin. The reaction catalyzed by 6,7-dimethyl-8-ribityllumazine synthase can proceed without enzymatic catalysis under physiological conditions. *J. Org. Chem.* **66**, 2555–2559.
39. Chenna, R., Sugawara, H., Koike, T., Lopez, R., Gibson, T. J., Higgins, D. G. & Thompson, J. D.

Please cite this article as: Klinke, S. *et al.*, Structural and Kinetic Properties of Lumazine Synthase Isoenzymes in the Order Rhizobiales, *J. Mol. Biol.* (2007), doi:10.1016/j.jmb.2007.08.021

(2003). Multiple sequence alignment with the Clustal series of programs. *Nucleic Acids Res.* **31**, 3497–3500.
40. Laskowski, R. A., MacArthur, M. W., Moss, D. S. & Thornton, J. M. (1993). PROCHECK: a program to check the stereochemical quality of protein structures. *J. Appl. Crystallogr.* **26**, 283–291.
41. Vagin, A. A., Richelle, J. & Wodak, S. J. (1999). SFCHECK: a unified set of procedure for evaluating the quality of macromolecular structure-factor data and their agreement with atomic model. *Acta Crystallogr. Sect. D: Biol. Crystallogr.* **55**, 191–205.
42. Krissinel, E. & Henrick, K. (2004). Secondary-structure matching (SSM), a new tool for fast protein structure alignment in three dimensions. *Acta Crystallogr. Sect. D: Biol. Crystallogr.* **60**, 2256–2268.
43. Kraulis, P. J. (1991). MOLSCRIPT: a program to produce both detailed and schematic plots of protein structures. *J. Appl. Crystallogr.* **24**, 946–950.
44. Merritt, E. A. & Bacon, D. J. (1997). Raster3D: photorealistic molecular graphics. *Methods Enzymol.* **277**, 505–524.
45. Pettersen, E. F., Goddard, T. D., Huang, C. C., Couch, G. S., Greenblatt, D. M., Meng, E. C. & Ferrin, T. E. (2004). UCSF Chimera—a visualization system for exploratory research and analysis. *J. Comput. Chem.* **25**, 1605–1612.
46. Baker, N. A., Sept, D., Joseph, S., Holst, M. J. & McCammon, J. A. (2001). Electrostatics of nanosystems: application to microtubules and the ribosome. *Proc. Natl. Acad. Sci. USA*, **98**, 10037–10041.

Please cite this article as: Klinke, S. *et al.*, Structural and Kinetic Properties of Lumazine Synthase Isoenzymes in the Order Rhizobiales, *J. Mol. Biol.* (2007), doi:10.1016/j.jmb.2007.08.021